

Distribution of Convective Lower Halocline Water
In the Eastern Arctic Ocean

Takashi Kikuchi, Kiyoshi Hatakeyama,

Japan Marine Science and Technology Center

2-15, Natsushima-cho, Yokosuka, 237-0061, JAPAN

and

James H. Morison

PSC/APL, University of Washington

Seattle, WA 98105-6698, U.S.A.

Submitted to JGR-Oceans on Nov.21 2003

Revised on May 31, 2004

Abstract

We investigate the distribution of convectively formed Lower Halocline water (cLHW) in the eastern Arctic Ocean using observational and climatological data. The cLHW can be defined as the water mass in the cold halocline layer formed by winter convection. The presence of cLHW is indicated by temperatures close to the freezing point and a sharp bend in the Θ -S curve near the salinity of cLHW. Results from ice drifting buoy observations in 2002 show differences in water mass characteristics in the upper ocean among the Amundsen Basin, over the Arctic Mid Ocean Ridge, and in the Nansen Basin. In 2000-2002 cLHW was present over the Arctic Mid Ocean Ridge and the Nansen Basin, but was largely absent from the Amundsen Basin. Using climatological data, we find that cLHW was confined to the Nansen Basin prior to 1990. In the early 1990s, cLHW still covered only the Nansen Basin, but extended to the northern side of the Arctic Mid Ocean Ridge in the mid 1990s and covered the whole of the Amundsen Basin by the late 1990s. In the early 2000s, the area of cLHW moved back to its present boundary on the northern side of the Arctic Mid Ocean Ridge. These results correspond roughly to other changes in the Arctic Ocean circulation and water mass structure, but with a time delay. We hypothesize that general circulation changes and the cutoff of source water for advective-convective modification of the LHW are causes of the change in cLHW distribution. The lag in changes to cLHW distribution behind other changes in the atmosphere and upper ocean are likely related to differences in circulation change with depth and the transit time from cLHW formation.

1. Introduction

Evolution of the Cold Halocline Layer (CHL) in the Arctic Ocean has been an important topic among Arctic oceanographers over the past few decades because the cold halocline prevents upward heat flux from the warm Atlantic water and thus helps maintain the sea ice cover. Earlier articles have argued that offshore advection of dense water produced by sea ice formation over the Arctic shelves plays an important role in formation of the cold halocline [e.g., *Aagaard et al.*, 1981; *Melling and Lewis*, 1982; *Jones and Anderson*, 1986]. Using this concept of the "Advective" Cold Halocline, many studies have sought to understand the contribution of dense shelf water to the cold halocline using *in situ* data, satellite data [e.g., *Martin and Cavalieri*, 1989; *Cavalieri and Martin*, 1994] and numerical methods [e.g., *Killworth and Smith*, 1984].

Other articles have proposed a convective mechanism for the formation of the CHL, especially in the eastern Arctic Ocean. *Rudels et al.* [1996] showed evolution of the cold halocline from the shelf toward the basin and explained the observational results in the eastern Arctic Ocean in terms of the "Convective" Cold Halocline. The mechanism includes the two important processes; one is deep winter convection that forms the cold salty water of the cold halocline, and the other is subsequent fresh water input by sea-ice melt or low salinity shelf water. The most saline water of the cold halocline, i.e., Lower Halocline Water, can be formed by winter convection through this mechanism, and in such a case can be called "convective" Lower Halocline Water (cLHW). *Steele and Boyd* [1998] combined the advective and convective mechanisms to explain oceanographic conditions observed in the eastern Arctic Ocean during the submarine-based Scientific Ice Expedition (SCICEX) cruises of 1993 and 1995. *Woodgate et al.* [2001] presented results from moorings and CTD observations across the shelf break region north of the Kara Sea, the Laptev Sea, and the East Siberian Sea. Offshore CTD results indicated the condition characteristic of a convective

cold halocline, a sharp bend in the temperature-salinity plots near the freezing point and at salinities near 34.0-34.4, but the cold halocline water was warmer and saltier in the near-shore ends of the sections. Altogether the mooring results suggested that the convective process was local and played an important role in forming the cold halocline in the eastern Arctic Ocean.

Steele and Boyd [1998] also discussed interannual variability of the cold halocline in the Arctic Ocean based on a comparison of new observations with climatological data and concluded that a remarkable salinization of near surface water during the mid 1990s produced a retreat of the cold halocline in the mid-Eurasian Basin. Recent papers [*Bjork et al.*, 2002; *Boyd et al.*, 2002] indicate a partial recovery of the cold halocline in recent years. As an indicator of the cold halocline strength, these papers focused on the change in near-surface salinity and its effect. However, enhanced near-surface salinization is still observed in the Amundsen Basin [*Morison et al.*, 2002] and continues to be an important signal of change in the Arctic.

How the cLHW properties and distribution change during the retreat and recovery of the cold halocline is largely unknown. In this article, we use observations to examine the difference in water mass characteristics among the basins in the eastern Arctic Ocean and clarify the distribution of the cLHW and its interannual variability in the eastern Arctic Ocean. Data from JAMSTEC (Japan Marine Science and Technology Center) Compact Arctic Drifter (J-CAD) ice-drifting buoys, climatological data, and historical data are used for this study. Details of the data are presented in Section 2. Analysis using J-CAD buoy number 4 (J-CAD 4) is described in Section 3. Based on these results, we investigate the distribution of the cLHW using the climatological data and historical observations in Section 4. We give our conclusion and discussion in section 5.

2. Data

We deploy the J-CAD buoys to understand the structures of ocean currents and water properties under the multi-year ice of the Arctic Ocean. Development of the buoys began in 1999 in collaboration with MetOcean Data System Limited [*Hatakeyama and Monk, 2001*]. We have deployed J-CAD buoys near the North Pole as part of the North Pole Environmental Observatory every year since 2000 [*Morison et al., 2002*]. The details of buoy technology, data sampling in the Arctic Ocean, and data processing are described in the J-CAD Data Report [see *Kikuchi and Hosono, 2004*]. The J-CAD buoys sample a broad suite of oceanographic and atmospheric parameters once per hour, yielding good spatial resolution for typical ice velocities. Position is determined by the Global Positioning System (GPS) and data are telemetered using the Argos and ORBCOMM systems

In this article, we mainly use J-CAD 4 data to show the condition of the upper ocean in the eastern Arctic Ocean. J-CAD 4 was installed near the North Pole (88.51°N, 76.93°E) on April 26, 2002. Figure 1 shows the drift trajectory of J-CAD 4 from the Amundsen Basin to the Greenland Sea. The buoy drifted across the Amundsen Basin, the Arctic Mid Ocean Ridge (AMOR), the Nansen Basin, and the Yermak Plateau, and toward the Greenland Sea. During this drift J-CAD 4 collected more than 7300 samples from each of its sensors, and given the average ice velocity, these result in a horizontal resolution better than 150 m. Six Sea-Bird SBE37IM micro-Cat conductivity-temperature sensors were suspended from J-CAD 4 at the nominal depths of 25, 50, 80, 120, 180, and 250m. Actual sensor depths are corrected for cable motion by linear interpolation of corrections determined from pressure measurements made with the micro-Cats at 120 and 250 m depth. J-CAD 1 and 3 were also deployed near the North Pole in April 2000 and April 2001, respectively. These data, with the addition of the CTD data of NPEO airborne surveys 2000-02 [*Morison et al., 2002*], are used to show water mass characteristics in the eastern Arctic Ocean prior to 2002.

Table 1 shows data sampling periods and locations of historical observations from 1991 to the present that are also used in this study. These data include observations from the *Oden* '91 cruise [Anderson *et al.*, 1994], Polar Ocean Profile (POP) buoy observation (Argos ID #12798) [see EWG, 1998; Morison *et al.*, 1982; Steele and Morison, 1992], the submarine observations of SCICEX 1993 and 1995-2000 [e.g., Morison *et al.*, 1998; Steele and Boyd, 1998; Smethie. *et al.*, 2000; Gunn and Muench, 2001].

3. Observations in 2002

Figure 2 shows the section of salinity versus latitude observed by J-CAD 4 in 2002 and the bottom topography along the J-CAD 4 trajectory. Frontal structures are apparent at about 87°N, 85°N, and 82.8°N. The front at 87°N is located between the Amundsen Basin and the AMOR. Relatively fresh water (salinity less than 34.0) is found only in the surface layer on the Amundsen Basin side of the AMOR. The front at 85°N is between the AMOR and the Nansen Basin. The front at 82.8°N is between the Nansen Basin and the Yermak Plateau. Temperature and salinity increased at 120 m, 180 m, and 250 m as J-CAD 4 proceeded across the fronts southward. These frontal structures indicate that the water mass characteristics are different in the Amundsen Basin, over the AMOR, in the Nansen Basin, and over the Yermak Plateau.

Figure 3 presents potential temperature-salinity (Θ -S) diagrams illustrating the differences in water mass characteristics among in the Amundsen Basin, over the AMOR, and in the Nansen Basin. The plus marks, "+", show the mean value of Θ and S at 180 m and 250m in each region. Both Θ and S at 180 and 250 m depths increase from the Amundsen Basin through the AMOR to the Nansen Basin. For example, averaged salinity and potential temperature at 250 m depth in the Amundsen Basin and the Nansen Basin are (34.86, 1.54)

and (34.91, 1.85), respectively. This suggests that water in the Amundsen Basin has traveled farther from the Atlantic Ocean than water in the Nansen Basin. Another difference in the water mass characteristics among these regions that is critical to this paper is the nature of the bend in the Θ -S curves separating the lower salinity, near-freezing surface layers and thermocline waters. This bend appears in a salinity range of 34.0 to 34.4. Considering the Θ -S structure of the Arctic Ocean as a whole, water with these salinity and temperature characteristics are commonly found overlain with cold, lower salinity waters of the halocline and are referred to as Lower Halocline Water. (LHW). The fact that they are found near the surface suggests that the measurements are in the region where LHW may be formed by surface processes before being subducted below fresher waters. In the Amundsen Basin, the temperature at the LHW bend is above the freezing point and the salinity is about 34.2. In contrast, the temperature of the LHW bend over the AMOR and in the Nansen Basin is close to the freezing point and the salinity is higher than in the Amundsen Basin. Therefore, we postulate that the shape of the LHW bend and other differences in water properties in the depth region of the LHW are associated with differences in the cold halocline formation process.

To compare the halocline formation mechanisms among these regions, we consider two basic cold halocline formation processes based on the schemes of *Rudels et al.* [1996] and *Steele and Boyd* [1998]. The earliest explanation for the formation of the cold halocline was that of *Aagaard et al.* [1981]. They proposed that the cold halocline water could be formed by an advective mechanism of lateral intrusion and mixing at depth of Atlantic-derived shelf water alternately freshened by river runoff and cooled to freezing and increased in salinity by ice formation. *Rudels et al.* [1996] proposed a convective scheme for formation of the cold halocline. *Steele and Boyd* [1998] explored the convective mechanism and proposed further modification to the cold halocline by an advective-convective mechanism. They argued that

only in the Barents Sea does the shelf water have high enough salinity to intrude at the depth of the LHW. Using temperature and salinity information alone it would be impossible to distinguish between the results of the advective and advective-convective mechanism, but the geographic context of our results will suggest that the convective and advective-convective mechanisms are dominant. Figure 4 and 5 are schematic views of the cold halocline formation by the convective [*Rudels et al.*, 1996] and advective-convective [*Steele and Boyd*, 1998] mechanisms, respectively.

Following *Rudels et al.* [1996], Figure 4 starts in the first panel with an initial condition representing the inflow of Atlantic Water (AW) into the basin in the Fram Strait branch. The surface has been freshened and cooled by interaction with the atmosphere to the freezing point. We call this surface end member preexisting Surface Water (pSW). The corresponding Θ -S curves form a straight line between pSW and AW. This corresponds to the solid lines in the Θ -S diagrams of Figure 3 drawn by crossing the two "+" marks at the mean Θ and S for 180 m and 250 m. The second panel illustrates the situation after ice formation. Because stratification of the initial profile is weak, unstable convection under the growing ice forms a deep (e.g., 100 m), more saline mixed layer at the freezing point. The characteristic segment in the corresponding Θ -S diagram is from the Θ -S just below the base of the new mixed layer, down a line of constant density to the freezing point line at the mixed layer salinity. As illustrated in the third panel, when ice melts it produces a shallower summer mixed layer. In the Θ -S this appears as a segment toward lower salinity on the freezing point line. If subsequent ice formation is as strong (produces as much instability) as the initial freeze-up, the summer mixed layer will mix down to the permanent pycnocline. *Rudels et al.* [1996] proposed that the addition of fresh shelf water would inhibit full mixing. This is likely a factor in many regions and is the essence of the *Steele and Boyd* [1998] advective-convective mechanism. However, in an idealized situation it is not necessary.

The greatest exposure to freezing conditions is likely to occur near where Atlantic Water first enters the Arctic sea ice cover in winter. Here the stratification is lowest and the rates of heat loss are likely to be high (e.g., Whaler's Bay north of Svalbard). Subsequent freeze cycles will occur over the Atlantic water after it travels farther east in the Amundsen Basin and will likely start from a lesser percentage of open water. Consequently, they will likely not cause convection to a depth as great as the first freeze cycle. The result after several freeze-melt-freeze cycles could look like the fourth panel. A stepped halocline structure at the freezing point down to a thermocline coinciding with a sharp, maximally deep halocline structure. Thus, a cold halocline can be formed solely by the convective process.

The consequence of refreezing in Θ -S space (Θ -S plot of Fig. 4d) is only that the endpoint will move back to a greater salinity on the freezing point line. The sharp LHW bend characteristic of the convective mechanism remains. The Θ -S curve for water deeper than the LHW lies along a constant density line through the LHW salinity near the freezing point. This means that the temperature of the LHW is close to the freezing point, and that at the top of the main thermocline the temperature is lower and the salinity higher than the mixing line between the pSW and AW. It is noteworthy that mixed layer water likely does not move with the deeper Atlantic water, but often in opposition to it. This near-surface layer freshened by convective and advective processes all over the basin tends to shield the deep halocline from any type of vertical mixing and supports the maintenance of a sharp LHW bend in the Θ -S diagram at the base of the cold halocline (Fig. 4d)

Figure 5 illustrates the advective-convective mechanism of *Steele and Boyd* [1998]. Here, shown in gray in the first panel, we start with pSW in a convectively formed mixed layer at the freezing point. The Θ -S characteristics are the same as for the convective mechanism (Fig. 4a). In the second panel (Fig. 5b) fresher water at the freezing point is advected in over this layer and mixes to some extent with the whole convectively formed layer. The effect on

the Θ -S curve is much different than in the case of the convective mechanism. The temperature at the LHW bend does not remain at the freezing point. The Θ and S at the bend are on the mixing line between pSW and AW and the bend has a large radius compared to the convective case. It is notable that while *Steele and Boyd* [1998] indicate the fresh, freezing-point surface water comes from the shelves, it could as described above come from another part of the basin freshened by summer melting of ice or Pacific-derived water. The mechanism is the same and the distinguishing gradual LHW bend with temperature elevation above freezing at the bend is the same.

Comparing the observed Θ -S curve with the mixing line in Figure 3(a) shows the temperature of the LHW to be greater than the freezing point for buoy data from the Amundsen Basin. The situation is similar to the case of advective-convective formation idealized in Figure 5. On the other hand, the Θ -S curves from buoy data gathered over the AMOR (Fig. 3b) and in the Nansen Basin (Fig. 3c) resemble the idealized depiction of convective cold halocline formation (Fig. 4d). The LHW bend is sharper and the Θ -S points lie close to a constant density line at the top of the main thermocline. The temperature of the Lower Halocline Water is near the freezing point. This suggests that for the water found over the AMOR and in the Nansen Basin, convective cold halocline formation has occurred before freshwater input near the surface layer and has not been modified by subsequent advective processes or melt-freeze cycles.

4. Interannual variability of the cLHW distribution

To examine the interannual variability in the distribution of the convectively formed LHW (cLHW) it is useful to quantify the characteristic shape of the Θ -S diagram in the region of the LHW bend. The arguments above indicate the cLHW bend should be sharp and the

temperature of cLHW should be near the freezing point. These properties correspond to the typical convective case shown in Figure 4. From the results of J-CAD 4 observations (Figure 3), we can estimate the salinity of pSW from the point where the solid line and the freezing temperature line intersect. The value is about 34.1. If cLHW is present, temperature at the salinity of the pSW should be close to the freezing point. If the advective-convective or advective processes form the LHW, the temperature at the salinity of the pSW should be above the freezing point. Therefore, we can use the temperature above the freezing point, or freezing temperature departure (FTD), on the 34.1 salinity surface to detect the distribution of cLHW. There are other approaches to illustrate the distribution of cLHW, e.g., salinity at the LHW bend of Θ -S curve. However, it is sometimes difficult to define the bend depth based on discrete salinity and temperature data from drifting buoys or historical Nansen bottle data at standard depths, whereas interpolating to a particular salinity is usually straight forward and avoids errors associated with depth estimation. A salinity of 34.1 is representative of pSW as extrapolated from the Atlantic Water mixing line throughout the eastern Arctic Ocean. Earlier observational and climatological data show similar Θ -S curves and produce similar estimates of pSW salinity in the eastern Arctic Ocean. We checked the distributions of FTD for salinities between 34.0 and 34.4 and compared the corresponding shapes of the Θ -S curves. We found that for J-CAD 4 data showing evidence of cLHW, the FTD never rises to 0.2°C in the 34.0 to 34.4 salinity range, even in the summer season [e.g., *McPhee et al.*, 2003]. We also found the average value of pSW salinity to be 34.1 in the eastern Arctic Ocean. From these results we concluded that for the purposes of analyzing historical data, an FTD less than 0.2°C at a salinity of 34.1 is indicative of a sharp LHW bend and the presence of cLHW. Because this temperature threshold appears relatively insensitive to temperatures within the likely range of pSW salinities, the “ 0.2°C at a salinity of 34.1” criteria should be robust to local differences in pSW salinity.

Figure 6 presents the distribution of FTD on the 34.1 salinity surface from the observational results in the early 2000s. The data were obtained from NPEO airborne surveys in 2000-2002 and the SCICEX 2000 cruise in addition to J-CAD observations. The thick dotted line shows $FTD=0.2^{\circ}\text{C}$ at a salinity of 34.1, which as discussed above, we define as the upper FTD boundary of cLHW. This line was between the Amundsen Basin and the AMOR in the early 2000s implying that cLHW was prevalent in the AMOR and the Nansen Basin but not the Amundsen Basin during this time.

Figure 7 illustrates distributions of FTD on the salinity 34.1 surface north of 75°N from the EWG winter climatology [EWG, 1997]. The data were collected between 1948 and 1993. The FTD on the 34.1 salinity surface in the southern half of the Nansen Basin is below 0.2°C , indicative of the presence of cLHW. The area of the cLHW extends from the Nansen Basin to near Severnaya Zemlya ($\sim 100^{\circ}\text{E}$) and into the Kara Sea. FTD becomes close to 0.3°C over the AMOR and off the Laptev Sea. The FTD in the Amundsen Basin is much higher than over the AMOR and in the Nansen Basin. The water properties over the Siberian side of the Lomonosov Ridge and off the western side of the East Siberian Sea are similar to those in the Amundsen Basin.

The comparison of Figures 6 and 7 shows that in 2000-2002 the distribution of cLHW was more extensive than climatology. At least for the region for which we have data in 2000-2002, the area of cLHW extended farther, to the northern side of the AMOR, than the pre-1990 climatology. Also, the FTD in the Amundsen Basin in 2000-2002 was much lower than the climatology.

In previous papers the mid-1990s weakening of the cold halocline was characterized mainly by increased salinity in the upper ocean, typically just below the nominal mixed layer depth [Steele and Boyd, 1998; Bjork et al., 2002; Boyd et al., 2002]. Little attention was

given to quantitative indication of the distribution of cLHW. By examining the FTD at the 34.1 salinity surface in data from the 1990s in the eastern Arctic Ocean, we find that the cLHW distribution became most extensive in the late-1990s.

Figure 8 illustrates the distributions of FTD on the 34.1 salinity surface in a) the early 1990s (1991-93), b) the mid 1990s (1994-1996), and c) the late 1990s (1997-1999). The thick blue lines correspond to FTD on the 34.1 salinity surface equal to 0.2 as in Figure 6. In the early 1990s cLHW occurred only in the Nansen Basin (Fig. 8a), extending only slightly closer to the AMOR than in the climatology (Fig. 7). The area of cLHW extended to the northern side of the AMOR in the mid-1990s (Fig. 8b) and advanced further to cover the whole Amundsen Basin in the late 1990s (Fig. 8c). Our data (Fig.6) indicates that since the early 2000s the distribution of cLHW has retreated to the Nansen Basin and AMOR.

According to previous articles, the variability of the Cold Halocline since the 1990s appeared as a change of upper ocean salinity in the eastern Arctic Ocean [e.g., *Steele and Boyd, 1998; Bjork et al., 2002; Boyd et al., 2002*]. They argue that the region freshened by runoff moved from the AMOR toward the Makarov Basin during the 1990s. More recent papers [*Bjork et al., 2002; Boyd et al., 2002*] argue it has spread back into the Amundsen Basin since 1999. In terms of formation mechanism, the issue is confused somewhat by the use of salinity as the indicator of cold halocline strength because others [e.g., *Carmack et al., 1995; McLaughlin, 1996; Jones et al., 1998; Morison et al., 1998*] argue the salinity increase in the Makarov Basin was due to a retreat of Pacific-derived waters and advance of Atlantic-derived waters. *Morison et al., [2002]* indicate that as late as 2000 the Pacific-derived waters had actually drawn back farther toward Canada than found by *Jones et al. [1998]* in 1994. The sharpness of the LHW bend, or FTD on the 34.1 salinity surface, as an indicator of cLHW is independent of the surface salinity criteria of cold halocline strength and unaffected by the questions of salt source. The interannual variability of cLHW is

similar but slightly different from the change in surface salinity distribution since 1990s.

The distribution of cLHW is slightly different from the surface salinity distribution probably because its presence indicates a lack of exposure to reduced salinity water (advective-convective mechanism) or similar density water at elevated temperature water (advective mechanism) over the whole previous trajectory of LHW.

5. Summary and discussion

We examine water mass characteristics in the eastern Arctic Ocean and use observational and climatological data to determine the prevalence and interannual variability of the convectively formed Lower halocline Water (cLHW). In the early 2000s, the water mass characteristics were different among in the Amundsen Basin, over the Arctic Mid Ocean Ridge, and in the Nansen Basin. These differences show evidence of cLHW over the AMOR and in the Nansen Basin but not in the Amundsen Basin in the early 2000s.

The convective formation process that creates cLHW [Rudels *et al.*, 1996] is shown in Figure 4, and the advective-convective process [Steele and Boyd, 1998] is shown in Figure 5. The advective formation of the CHL proposed by Aagaard *et al.* [1981], involves interleaving of cold salty water from the shelves with halocline water at depth. Some papers have shown such interleaving of the cold salty water over the continental shelf of the Barents Sea [e.g., Steele *et al.*, 1995]. Though our method can not distinguish between advective-convective and advective LHW formation, it does detect cLHW as distinct from either of these, and for climatology, the 1990s and the 2000-2002 data we see only cLHW in the Nansen Basin adjacent to the Barents Sea. This suggests any advective or advective-convective LHW formation must originate farther east into the Arctic Ocean. Steele and Boyd [1998] argue that the salinity on the shelves is only high enough to produce advective formation in the Barents Sea and that advective formation must therefore be rare. We find that in the

climatology (Figure 7) appropriate salinities and temperatures may occur on the shelf east of Severnaya Zemlya, but that cLHW occupies the Nansen Basin margin between Svalbard and Severnaya Zemlya. Therefore, our results also suggest that advective formation of LHW is rare.

Comparison of FTD on the 34.1 salinity surface in the EWG [1997] climatology, 1990s data and our NPEO data show the advance and retreat of the cLHW distribution since the early 1990s. In the early 1990s, the cLHW was found only in the Nansen Basin, similar to climatology. The area extended toward the north, and cLHW extended into the Amundsen Basin, the AMOR, and the Nansen Basin in the late 1990s. This variability of cLHW distribution is similar to the surface ocean salinity and circulation changes that featured more saline Atlantic-derived waters penetrating across the Lomonosov Ridge and into the Makarov basin. The unique thing about the change in cLHW distribution is that it unequivocally indicates that by the mid-1990s the advective and advective-convective formation processes had shutdown over the whole eastern Arctic Ocean, thus leaving cLHW, which likely still formed along the southern margins of the Nansen Basin, to spread undisturbed through the rest of the Nansen and Amundsen basins.

The CHL covers most of the Arctic Ocean, but recent studies suggested that "CHL was disappearing" [e.g., *Steele and Boyd, 1998; Bjork et al., 2002; Boyd et al., 2002*]. These studies used the presence of low salinity near-surface water as a signal of CHL and argued its interannual variability. The boundary between a presence and absence of low salinity surface water seems to correspond to that of cLHW presented here. Thus, the variability of CHL distribution might "mirror" or "reflect" that of the convective formation process represented by FTD determination of cLHW. It seems reasonable that the extent of cLHW might define a minimum extent of CHL because the convection process forms a strong cold halocline with temperatures forced right to the freezing point, and it may be that during

periods when other CHL formation processes are more important the thickness and strength of the CHL would bear less relation to the presence of the cLHW. On the other hand, it is hard to see how the low salinity signature of the CHL would arise reliably from the convective part of the process; salinity decrease is more directly associated the melting process and advective processes that don't reach the LHW. For example what happened in the CHL at 50-100 m may have been affected more by input of low salinity water to the surface layer. The increase in salinity marking the weakening of the cold halocline in other papers likely has much to do with disappearance of the advective effects (e.g., Russian River water moved to the east) that come after initial CHL convective formation. So the correspondence of the cLHW with the shallow salinity defined CHL may be there because the predominance of cLHW is associated with the decrease of the salinity-lowering, freshwater advection mechanism of the low shallow salinity defined CHL.

Interestingly and in contrast to 2000-2002, the 1990s showed FTD near zero over the whole Yermak Plateau (mid 90s, Fig. 8b) or around it where the Atlantic Water follows the bathymetric contours (early and late 90s, Figs. 8a and 8c). Given the results of *McPhee et al.* [2003] and others describing strong mixing over the Yermak Plateau, we might expect variations in FTD there to be the result of a change in the balance between convective mixing, which would be lower FTD at the 34.1 salinity surface, and mechanical mixing by tides and topographic effects that would mix Atlantic Water upward, thereby raising FTD.

There are two possible and non-exclusive causes for the change in cLHW distribution: circulation and freshwater source. Both of these relate to a change in the 1990s toward a more cyclonic atmospheric circulation as indicated by the Arctic Oscillation (AO) [*Thompson and Wallace, 1999*]. The AO index is an expression of the strength of the Northern Hemisphere atmospheric Polar Vortex. Rising wintertime AO is associated with lower surface atmospheric pressure and a more cyclonic circulation over the Arctic. Before the late

1980s, wintertime AO indices were relatively low on average and rose significantly after the late 1980s until the mid 1990s. The AO index shows a great deal of interannual variability, but on average it gradually decreased during the late 1990s. Now the wintertime AO index is lower than its peak in the mid-1990s but is still elevated above the pre-1990 average.

Numerous authors [e.g., *Proshutinsky and Johnson, 1997; Morison et al., 2000*] have related the cyclonic shift in ocean circulation and frontal structures in the 1990s to the increased cyclonic circulation of the atmosphere. The advance of the cLHW is likely in part a component of this circulation shift.

The shift to a more cyclonic atmospheric circulation also affects the sources of cold fresh surface water required for the advective-convective formation of LHW (Fig.5). *Steele and Boyd [1998]* proposed that the retreat of the cold halocline was due to the deflection of this source water on the Russian shelves, freshened by river runoff, to the east by the more cyclonic atmospheric circulation of the mid 1990s. A similar argument applies when we consider sea ice and mixed layer water as possible sources for advective-convective LHW formation. *Rigor et al. (2002)* examine the relation between sea ice motion and the AO and find that when the AO index is positive, sea ice motion in the eastern Arctic Ocean near the Kara Sea and Laptev Sea tends to be eastward or offshore [Figure 11 of *Rigor et al., 2002*] carrying the potential source water for advective-convective LHW formation away from where cLHW is formed at depths shallow enough to be reached by advective-convective formation. When the AO index is low the sea ice moves westward through the Nansen Basin toward the Fram Strait, directly to where cLHW occurs at depths shallow enough to be modified by advective-convective near-surface mixing.

There appears to be a time lag of several years between the increased cyclonic forcing and the spread of cLHW across the AMOR and Amundsen Basin. This is likely due to a lag in ocean circulation change and the delay between a change in the LHW formation

mechanism at the formation location and its appearance elsewhere. For example *Morison et al.* [2002] find that the signals of circulation change evident in the North Pole temperature have propagated slowly deeper with time, so that while the Atlantic core temperatures reached a maximum in 1995, the temperatures appear to still be increasing below the core. The cLHW is deep enough so that we can expect the baroclinic adjustment of the circulation at the depth could lag the changes in wind forcing considerably. The delay between any type of LHW formation and its appearance away from the formation site must reflect the transit time of the LHW around the basin. If the LHW follows the Atlantic Water eastward through the Nansen Basin and recirculates back through the Amundsen Basin we might expect a time delay of 2-3 years between cLHW formed in the western Amundsen Basin to reach the Amundsen Basin, in rough agreement with the lag we observe.

Acknowledgement

The deployment of J-CAD 1, 3, and 4 were carried out as part of the North Pole Environmental Observatory (NPEO) with U.S. support of the U.S. National Science Foundation grant OPP-9910305. We deeply indebted to Andy Heiberg, Dean Stewart, Roger Anderson, Sigrid Salo, Trevor Monk, and Hirokatsu Uno, for their efforts in NPEO logistic support and J-CAD operations. We thank Masuo Hosono and Ken-ichi Kato for their help on J-CAD data processing. We sincerely thank Koji Shimada, Shigeto Nishino, and Takatoshi Takizawa, who provided useful comments for this study. Discussions with Mike Steele and Motoyoshi Ikeda were very fruitful. Their comments and suggestions were much appreciated. Comments from two reviewers were very helpful for improving the manuscript. Most of historical observational data were obtained from the NPEO, SEARCH, and NSIDC (National Snow and Ice Data Center) web sites and the EWG (1997) CD-ROM. We sincerely appreciate the scientist who generously sheared their data for our research.

Reference

- Aagaard, K., L. K. Coachman, and E. C. Carmack, On the halocline of the Arctic Ocean, *Deep Sea Res., Part A*, 28, 529-545, 1981.
- Anderson L.G., G. Bjork, O. Holby, E.P. Jones, G. Kattner, K.P. Koltermann, B.Liljeblad, R. Lindegren, B. Rudels, and J. Swift, Water masses and circulation in the Eurasian Basin: Results from the Oden 91 expedition, *J. Geophys. Res.*, 99, 3272-3283, 1994.
- Bjork, G., J. Soderkvist, P. Winsor, A. Nikolopoulos, and M. Steele, Return of the cold halocline layer to the Amundsen Basin of the Arctic Ocean: Implications for the sea ice mass balance, *Geophys. Res. Lett.*, 29, doi:10.1029/2001GL014157, 2002.
- Boyd, T. J., M. Steele, R. D. Muench and J. T. Gunn, Partial recovery of the Arctic Ocean halocline, *Geophys. Res. Lett.*, 29, doi:10.1029/2001GL014047, 2002.
- Carmack, E.C., R.W. McDonald, R.G. Perkin, F.A. McLaughlin and R.J. Pearson, Evidence for warming of Atlantic water in the southern Canadian Basin of the Arctic Ocean: Results from the Larsen-93 Expedition, *Geophys. Res. Lett.*, 22, 1061–1064, 1995.
- Cavalieri, D. J., and S. Martin, The contributions of Alaskan, Siberian, and Canadian coastal polynyas to the cold halocline layer of the Arctic Ocean, *J. Geophys. Res.*, 99, 18,343-18,362, 1994.
- Environmental Working Group (EWG), *Joint U.S.-Russian Atlas of the Arctic Ocean for the winter Period* [CD-ROM], Natl. Snow and Ice Data Cent., Boulder, CO., 1997.
- Environmental Working Group (EWG), *Joint U.S.-Russian Atlas of the Arctic Ocean for the Summer Period* [CD-ROM], Natl. Snow and Ice Data Cent., Boulder, CO., 1998.
- Gunn J.T., and R.D. Muench, Observed changes in Arctic Ocean in temperature structure over the past half decade, *Geophys. Res. Lett.*, 28, 1035-1038, 2001.

- Hatakeyama, K., and T. Monk, Development and Deployment of a Compact Arctic Drifting Platform, *Sea Technology*, 42 (No.7), 37-47, 2001.
- Jones, E. P., and L. G. Anderson, On the origin of the chemical properties of the Arctic Ocean halocline, *J. Geophys. Res.*, 91, 10,759-10,767, 1986.
- Jones, E. P., L. G. Anderson, and J. H. Swift, Distribution of Atlantic and Pacific waters in the upper Arctic Ocean: Implications for circulation, *Geophys. Res. Lett.*, 25, 765-768, 1998.
- Kikuchi, T., and M. Hosono, JAMSTEC Compact Arctic Drifter Buoy Data, *CliC Ice and Climate News*, 5, 14-15, 2004.
- Killworth, P. D., and J. M. Smith, A one-and-a-half dimensional model for the Arctic halocline, *Deep Sea Res.*, 31, 271-293, 1984.
- Martin, S., and D. J. Cavalieri, Contributions of the Siberian shelf polynyas to the Arctic Ocean intermediate and deep water, *J. Geophys. Res.*, 94, 12,725-12,738, 1989.
- McLaughlin, F. A., E. C. Carmack, R. W. McDonald, and J. K. B. Bishop, Physical and geochemical properties across the Atlantic/Pacific water mass front in the southern Canada Basin, *J. Geophys. Res.*, 101, 1183–1195, 1996.
- McPhee, G. M., T. Kikuchi, J. H. Morison, and T. P. Stanton, Ocean-to-Ice Heat Flux at the North Pole Environmental Observatory, *Geophys. Res. Lett.*, 30, 24, 2274, doi:10.1029/2003GL018580, 2003.
- Melling, H., and E. L. Lewis, Shelf drainage flows in the Beaufort Sea and their effect on the Arctic Ocean pycnocline, *Deep Sea Res., Part A*, 29, 967-985, 1982.
- Morison, J.H., S. Burke, H. Steltner and R. Andersen, SALARGOS temperature-conductivity buoys, *Oceans 82 Conference Record*, 1255-1260, 1982.
- Morison, J.H., M. Steele, and R. Anderson, Hydrography of the upper Arctic Ocean measured from the nuclear submarine U.S.S. Pargo, *Deep-Sea Res.*, 45, 15-38, 1998.
- Morison, J.H., K. Aagaard, and M. Steele, Recent environmental change in the Arctic: A

review, *Arctic*, 53, 4, 2000.

Morison, J.H., K. Aagaard, K. K. Falkner, K. Hatakeyama, R. Moritz, J. E. Overland, D.

Perovich, K. Shimada, M. Steele, T. Takizawa, and R. Woodgate, North Pole

Environmental Observatory delivers early results, *EOS Transactions, American*

Geophysical Union, 83(33), 357,360-361, 2002.

Proshutinsky, A. and M. Johnson, Two circulation regimes of the wind-driven Arctic Ocean, *J.*

Geophys. Res., 102, 12,493-12,514, 1997.

Rigor, I. G., J. M. Wallace, R. L. Colony, Response of Sea Ice to the Arctic Oscillation, *J.*

Climate, 15, 26482663, 2002.

Rudels, B., L. G. Anderson, and E. P. Jones, Formation and evolution of the surface mixed

layer and halocline of the Arctic Ocean, *J. Geophys. Res.*, 101, 8807-8821, 1996.

Steele, M. and J.H. Morison, Obtaining smooth hydrographic profiles from a buoy deployed

in sea ice. *J. Oceanic & Atmospheric Technology*, 9, 1992.

Steele, M., J.H. Morison and T. Curtin, Halocline water formation in the Barents Sea, *J.*

Geophys. Res., 100, 881-894, 1995.

Steele, M., and T. Boyd, Retreat of the cold halocline layer in the Arctic Ocean, *J. Geophys.*

Res., 103, 10,419-10,435, 1998.

Smethie Jr., W.M., P. Schlosser, G. Bonisch, and T.S. Hopkins, Renewal and circulation of

intermediate waters in the Canadian Basin observed on the SCICEX 96 cruise, *J. Geophys.*

Res., 105, 1105-1121, 2000.

Thompson, D. W. J., and J. M. Wallace, The Arctic Oscillation signature in the wintertime

geopotential height and temperature fields, *Geophys. Res. Lett.*, 25, 1297–1300, 1998.

Woodgate, R. A., K. Aagaard, R. D. Muench, J. Gunn, G. Bjork, B. Rudels, A. T. Roach, and

U. Schauer, The Arctic Ocean boundary current along the Eurasian slope and the adjacent

Lomonosov Ridge: Water mass properties, transports and transformations from moored instruments, *Deep Sea Res., Part I*, 48, 1757-1792, 2001.

Figure Caption

Figure 1. Drifting trajectory of J-CAD 4.

Figure 2. Meridional sections of (a) salinity observed by J-CAD 4 and (b) bottom topography below the buoy trajectory. Contour interval of Figure 2a is 0.1. AB: Amundsen Basin, AMOR: Arctic Mid Ocean Ridge, NB; Nansen Basin, YP: Yermak Plateau.

Figure 3. Potential temperature (Θ) - salinity (S) diagram for (a) Amundsen Basin, (b) Arctic Mid Ocean Ridge, (c) Nansen Basin. Colors show the depths of the data. Note that the plus marks (+) in the figures indicate mean value of potential temperature and salinity at 180 and 250 m depths. A solid line is drawn through both the plus marks in each figure. Thin lines with numbers between 27 and 28 show isopycnals. The dotted line shows the freezing point.

Figure 4. Schematic view of the formation process of the convective cold halocline in the eastern Arctic Ocean. Dotted lines of the lower panels show the freezing point. The labels for water types are pSW for pre-existing surface water, SW for surface water, cLHW for convectively formed Lower Halocline water, and AW for Atlantic water.

Figure 5. Schematic view of the formation process of the advective-convective cold halocline in the eastern Arctic Ocean as in Figure 4, but the label for for Lower Halocline water is LHW.

Figure 6. Distribution of Freezing Temperature Departure (FTD) on the 34.1 salinity surface in 2000-02. The data are from J-CAD, NPEO CTD observations, and SCICEX 2000 survey. The thick dotted line shows FTD=0.2°C. Contour lines show bottom topography with an interval of 500m.

Figure 7. Distribution of Freezing Temperature Departure (FTD) on the 34.1 salinity surface as in Figure 6, but the data are from mean winter climatology (EWG, 1997).

Figure 8. Distribution of Freezing Temperature Departure (FTD) on the 34.1 salinity surface

as in Figure 6, but the data were observed in (a) 1991-93, (b) 1994-96, and (c) 1997-1999.

Table 1. Sampling dates and locations of data used in this study

Ice-drifting buoy	Period and locations	
	(Start date and location)	(End date and location)
POP ID #12798	1993/09/01, 84.96N, 134.77E	to 1994/03/08, 88.85N, 91.76E
	1993/06/01, 88.03N, 26.77E	to 1994/11/23, 79.94N, 4.36E
J-CAD 1	2000/04/24, 89.68N, 134.33W	to 2000/11/01, 84.78N, 5.62E
	2000/11/28, 83.65N, 1.44W	to 2001/04/06, 68.22N, 18.09E
J-CAD 3	2001/04/08, 89.57N, 82.85E	to 2001/05/06, 89.29N, 5.06E
J-CAD 4	2002/04/26, 88.51N, 76.93E	to 2002/06/22, 72.39N, 10.94W
CTD/XCTD observation	(Start date and location)	(End date and location)
I/B Oden	1991/08/20, 83.56N, 27.63E	to 1991/10/03, 81.14N, 19.90E
SCICEX 93	1993/08/23, 89.99N, 146.84E	to 1993/09/13, 86.61N, 7.40E
SCICEX 95	1995/03/28, 73.53N, 160.93W	to 1995/05/08, 75.52N, 171.51E
SCICEX 96	1996/09/14, 78.14N, 169.27W	to 1996/10/28, 75.31N, 171.95W
SCICEX 97	1997/09/03, 84.25N, 26.30E	to 1997/10/02, 74.77N, 171.79W
SCICEX 98	1998/08/01, 75.28N, 176.99W	to 1998/09/01, 75.27N, 176.95W
SCICEX 99	1999/04/03, 74.29N, 160.55W	to 1999/05/10, 86.02N, 14.18E
NPEO 2000	2000/04/22, 89.68N, 138.77W	to 2000/04/28, 86.85N, 96.23W
SCICEX 2000	2000/10/17, 85.00N, 46.00E	to 2000/10/24, 75.23N, 175.32W
NPEO 2001	2001/04/09, 89.57N, 73.06E	to 2001/04/14, 89.47N, 54.72E
NPEO 2002	2002/04/23, 89.54N, 53.00E	to 2002/04/27, 86.62N, 164.99E

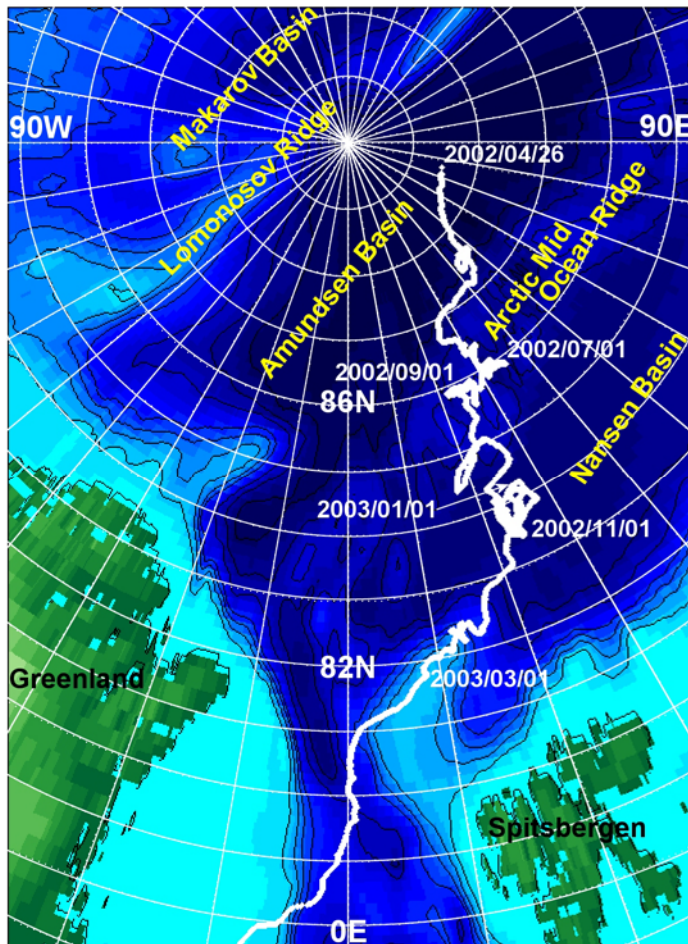


Figure 1. Drifting trajectory of J-CAD 4

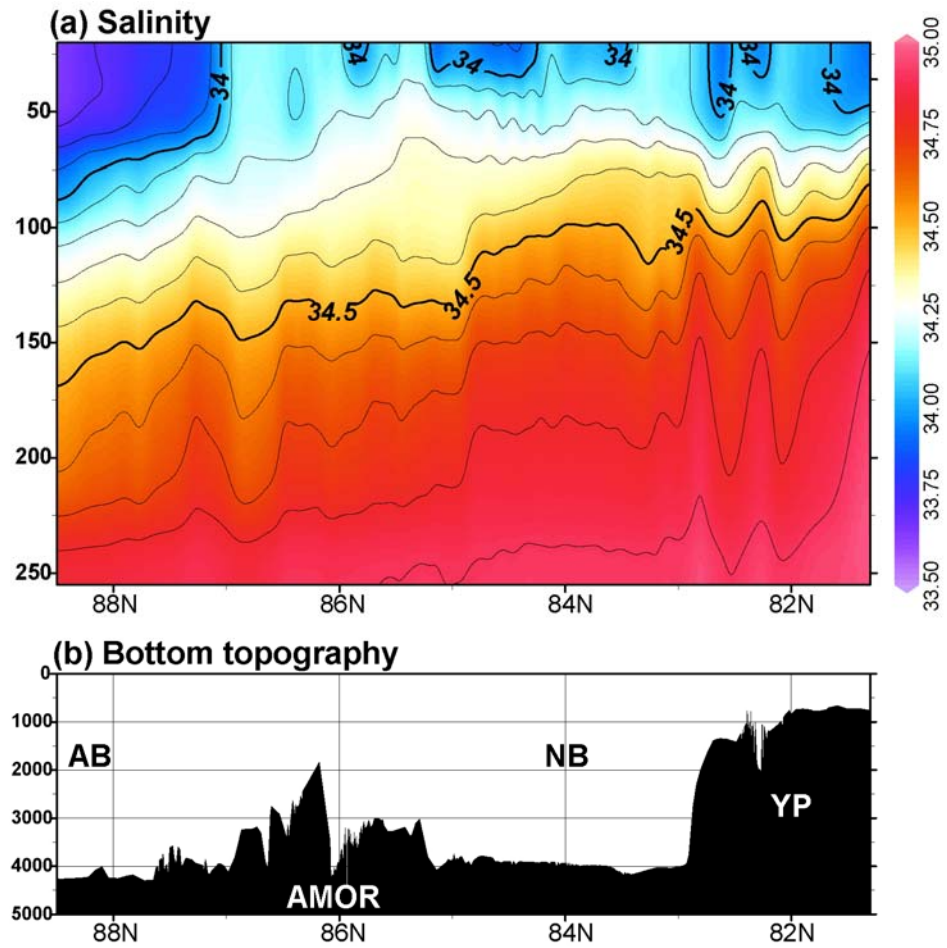


Figure 2. Meridional Section of (a) salinity observed by J-CAD 4 and (b) bottom topography below the buoy trajectory. Contour interval of Figure 2a is 0.1. AB: Amundsen Basin, AMOR: Arctic Mid Ocean Ridge, NB: Nansen Basin, YP: Yermak Plateau

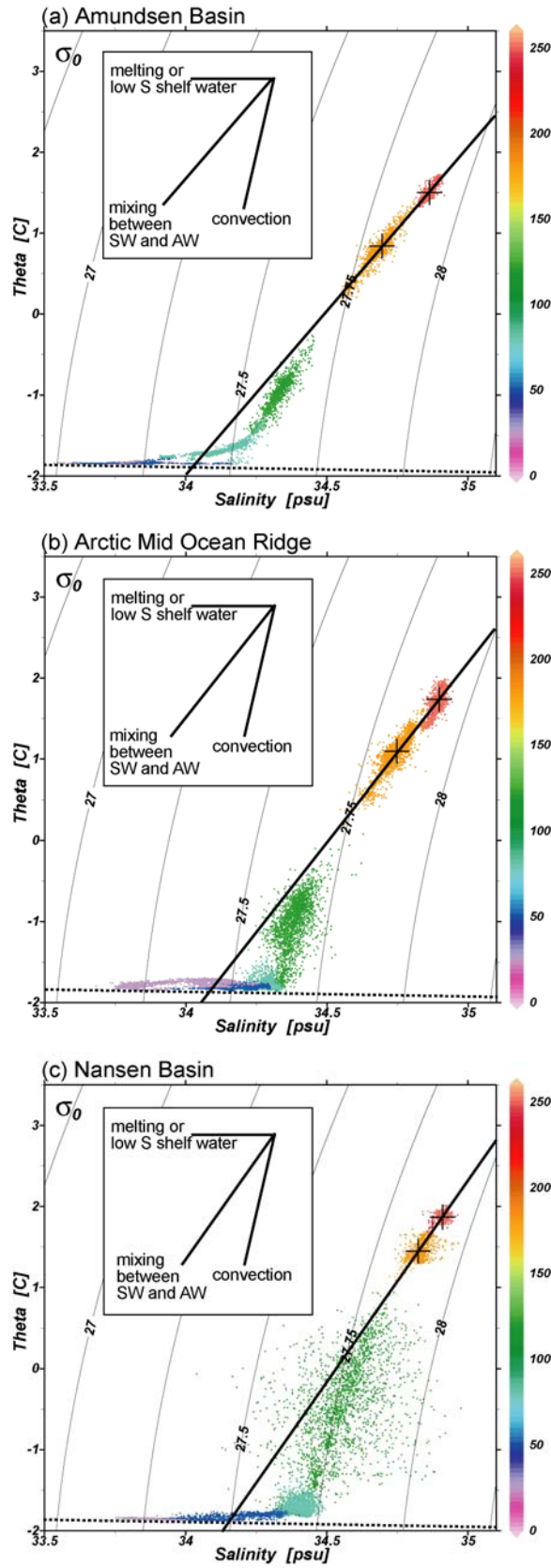


Figure 3. Potential temperature (Θ) - salinity diagram. Colors show the depths of the data. Note that the plus marks (+) in the figures indicate mean value of Θ and salinity at 180 and 250 m depths. Solid line crosses both the plus marks in each figure. Thin lines with number between 27 and 28 show isopycnals. Dotted line shows the freezing point. (a) Amundsen Basin, (b) Arctic Mid Ocean Ridge, (c) Nansen Basin

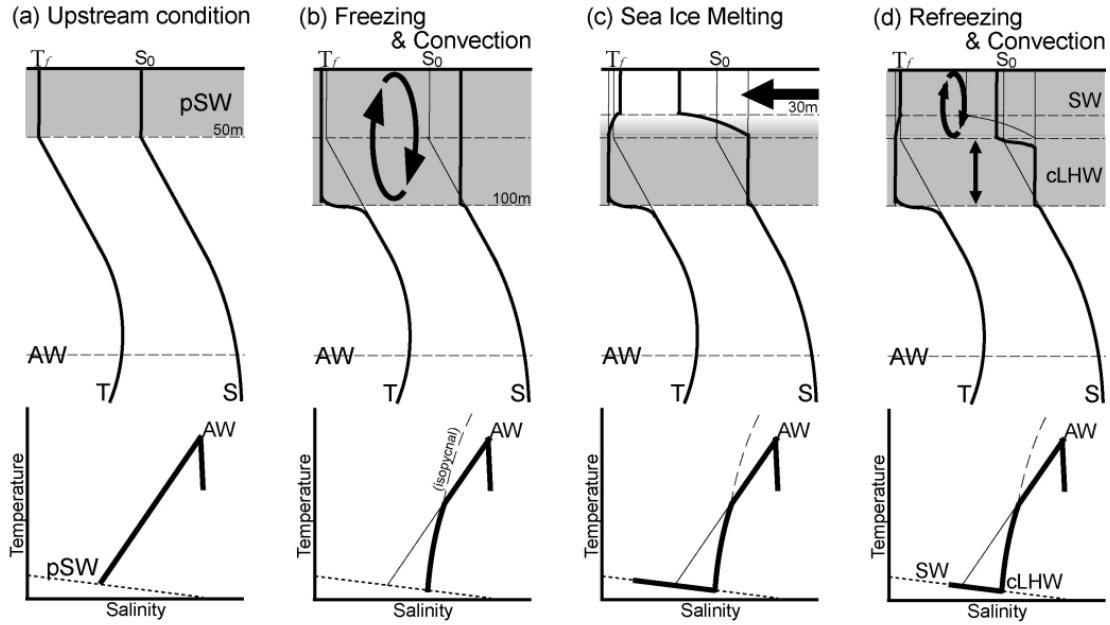


Figure 4. Schematic view of the formation process of the convective cold halocline in the eastern Arctic Ocean. Dotted lines of the lower panels show the freezing point. The labels for water types are pSW for pre-existing surface water, SW for surface water, cLHW for convectively formed Lower Halocline water, and AW for Atlantic water.

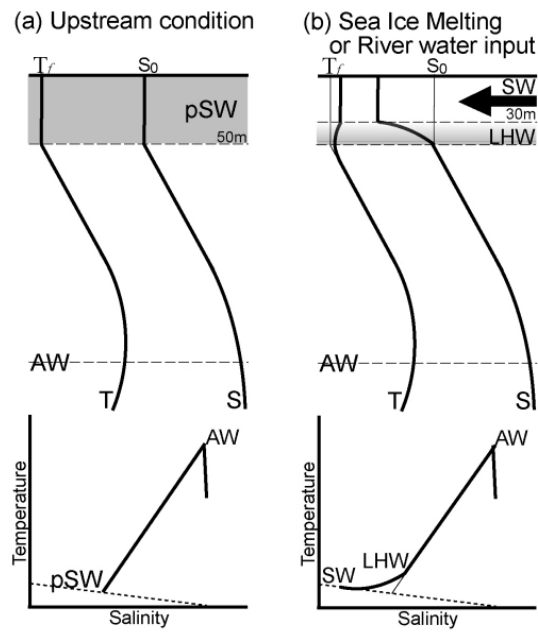


Figure 5. Schematic view of the formation process of the advective-convective cold halocline in the eastern Arctic Ocean as in Figure 4, but the label for water type is LHW for Lower Halocline water.

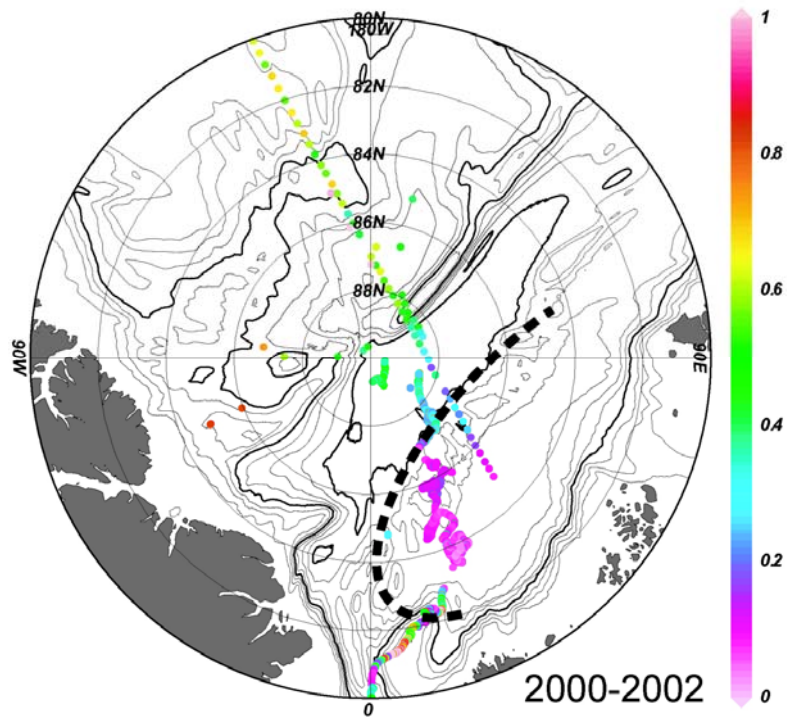


Figure 6. Distribution of Freezing Temperature Departure (FTD) on the 34.1 salinity surface in 2000-02. The data are from J-CAD, NPEO CTD observations, and SCICEX 2000 survey. The thick dotted line shows FTD=0.2. Contour lines show bottom topography with an interval of 500 m.

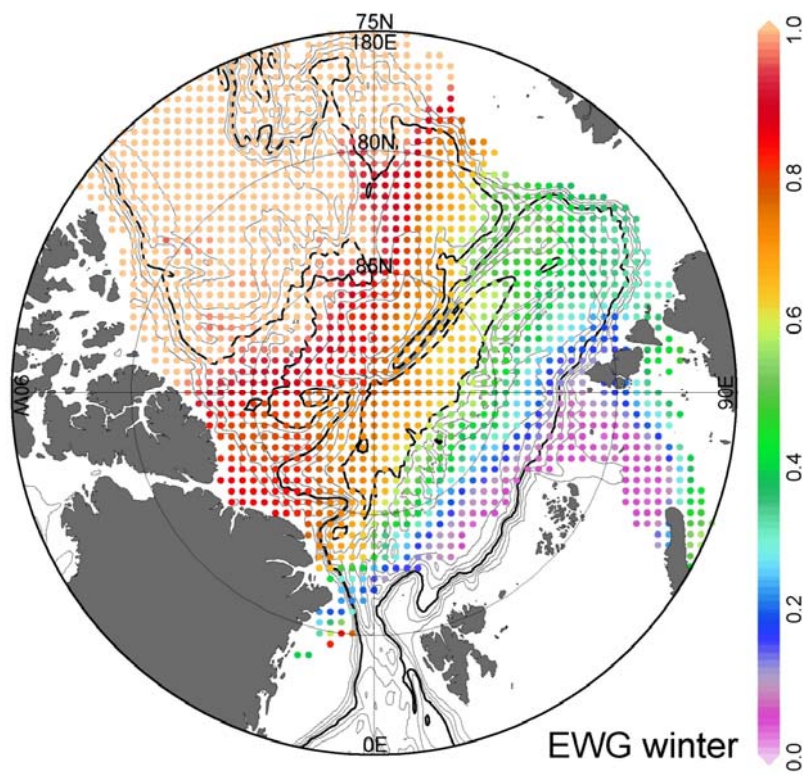


Figure 7. Distribution of Freezing Temperature Departure (FTD) on the 34.1 salinity surface as in Figure 6, but the data are from winter climatology (EWG, 1997).

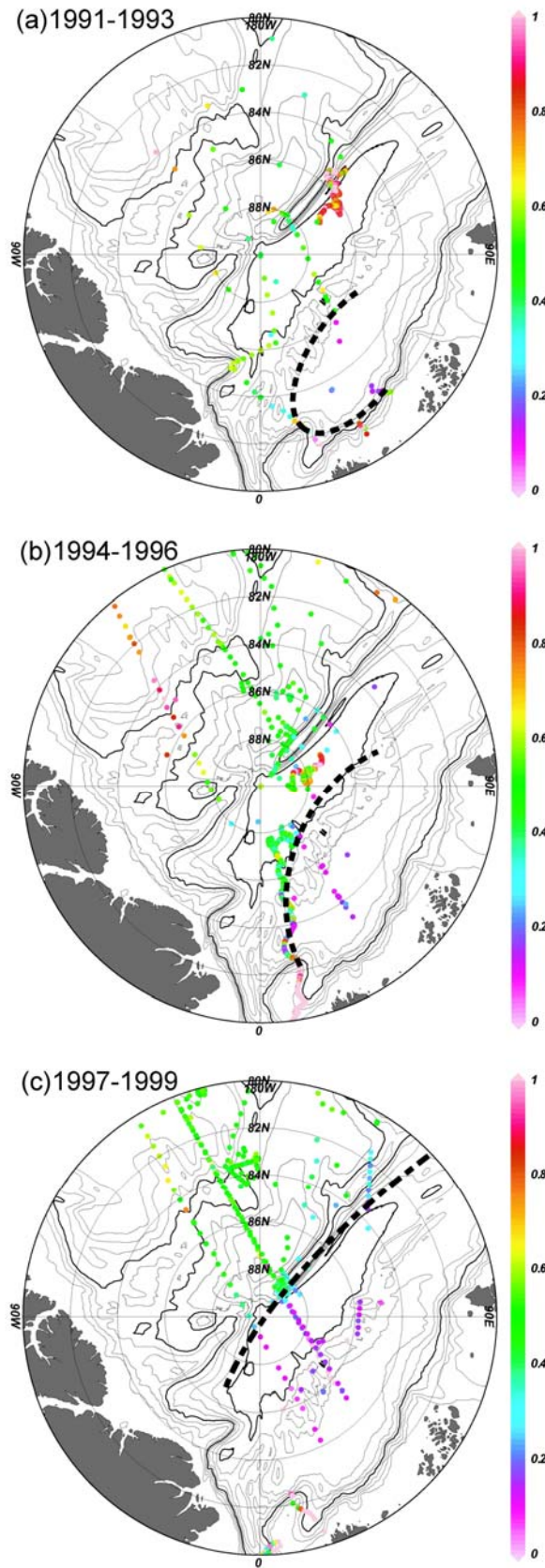


Figure 8. Distribution of Freezing Temperature Departure (FTD) on the 34.1 salinity surface as in Figure 6, but the data were observed in (a) 1991-93, (b) 1994-96, and (c) 1997-1999.